Computational Engineering and Physical Modeling 4-4 (2021) 39-63

Contents lists available at **CEPM**

Computational Engineering and Physical Modeling

Journal homepage: www.jcepm.com

Development of Dam-Break Model Considering Real Case Studies with Asymmetric Reservoirs

A. Ferdowsi[1,2], **M. Nemati**[2], **S. Farzin**[3*]

1. Lecturer, University of Applied Science and Technology, Tehran, 15996-65111, Iran

2. M.Sc. Graduate, Department of Water Engineering and Hydraulic Structures, Faculty of Civil Engineering, Semnan University, Semnan, Iran

3. Associate Professor, Department of Water Engineering and Hydraulic Structures, Faculty of Civil Engineering, Semnan University, Semnan, Iran

Corresponding author: saeed.farzin@semnan.ac.ir

https://doi.org/10.22115/CEPM.2021.311759.1188

ARTICLE INFO

Article history:
Received: 24 October 2021
Revised: 22 November 2021
Accepted: 22 November 2021

Keywords:
Dam-break;
Reservoir geometry;
Unsteady flow;
Computational fluid dynamics (CFD);
FLOW-3D.

ABSTRACT

Dam-break flow is known as one of the most horrible phenomena. Some hypothetical reservoir geometries were evaluated in literature, but in nature, each reservoir has a unique geometry. In the present research, dam-break flow was studied based on different reservoir geometries using FLOW-3D. Six reservoirs were considered: reservoirs R1 and R2 belonged to Mahabad Dam (Iran) and Tignes Dam (France), with asymmetric reservoirs, respectively; reservoirs R3 and R4 had symmetrical trapezoidal reservoirs with angles 30 and 45 degrees, respectively; reservoir R5 had a rectangular shape, extending from one side; and reservoir R6 had a long reservoir, which also was used to verify FLOW-3D. The model performance was verified by experimental results and FLUENT model in literature. Results showed FLOW-3D with mesh sizes 30×30×30 mm and k-ε turbulence model outperformed FLUENT, based on R2, RMSE, and MAE. The results of water levels and flow velocities at five points proved that dam-break flow could vary from one dam to another, considering reservoir geometry. Peak water levels and velocities have been measured to show how reservoir geometry could cause catastrophic flow.

How to cite this article: Ferdowsi, A., Nemati, M., & Farzin, S. (2021). Development of Dam-Break Model Considering Real Case Studies with Asymmetric Reservoirs. Computational Engineering and Physical Modeling, 4(4), 39–63. https://doi.org/10.22115/cepm.2021.311759.1188

1. Introduction

Dams are the most important hydraulic structures, which are built for serving various purposes including flood control, water supply, electricity production, recreation, navigation, artificial recharge of groundwater, and waste disposal; however, the failure of dams could have destructive impacts on human life [1], infrastructures and so on. Although studying the history of ancient Iran (Persia), Greece, Egypt, Iraq (Babylonia), Sri Lanka (Ceylon), China, India, and Roman, one can prove that the construction of these water works began thousands of years ago [2], but dam-break flow has remained unknown and also an interesting subject to study. A lot of dam breaks have occurred over the past century such as Gleno Dam in Italy, 1923; Saint Francis Dam in California, 1928; Malpasset Dam in France, 1959; and Teton Dam in Idaho, 1976 [3].

Modeling of hydraulic structures may be performed in laboratory [4,5] or using different methods such as numerical methods [6] or soft computing techniques [7–11]. In this regard, some studies were conducted to evaluate dam-break flow in different conditions. Bell et al. [12] experimentally attempted to investigate dam-break flow with unsteady flows in the straight and curved channels. Stansby et al. [13] studied dam-break flow regarding various downstream water heights. In recent years, by developing CFD methods, many attempts have been made to understand hydraulic behavior of dam-break flow according to the different conditions including various shapes of reservoirs, but none of them considered asymmetric reservoirs (in plan). Yang et al. [14] in an experimental study simulated cascade reservoirs in a channel with steep bottom slope to evaluate dam-break flow. The results showed that the flow behavior of dam-break flows in single and cascade reservoirs had some differences. Feizi Khankandi et al. [15] analyzed the effects of the geometry of reservoirs on dam-break flows. In this study, four different geometries of reservoirs, in plan, were employed such as long, wide, trapezoidal, and a model with a 90° bends. According to results, in some cases, the experimental models had the same results as the previous studies, but not all of them. Among all used reservoirs models, the wide reservoir model had the highest velocity and discharge values. In addition, the wide reservoir model had a sharper and narrower discharge curve. Farzin et al. [16] studied the unsteady 1-D dam-break flow problem. The MacCormack numerical scheme was used as a classical second order explicit scheme in the simulation of unsteady flow of dam-break phenomenon. The verification between the method and experimental results showed the method workability. Farzin et al. [17] used two types of novel smoothed particle hydrodynamics i.e., SPH methods to improve modeling wave propagation of incompressible flow during the dam-break. Also, OpenFoam software was used to compare the SPH with an Eulerian approach and the volume of fluid i.e., VOF. Results proved that both methods had very satisfying accuracy; however, the proposed SPH solving showed superior results based on consistency, stability, convergence, and pressure distribution. Farzin et al. [18] proposed a consistent implicit incompressible SPH method based on projection approach for solving problems of free surface flow. The validation of the proposed method (namely, ISPH) was performed in 2-D dam-break benchmarks, in both wet and dry beds. According to results, the proposed method performed well regarding different aspects, such as stability, number of particles, and also time steps. Wood and Wang [19] investigated dam-break flows in a numerical-experimental research. This study was performed to evaluate dam-break flows with different conditions in a channel with a 90° bend. Hooshyaripor et al. [20], in an experimental

investigation, studied instantaneous dam-failure flood based on different capacities and lengths of reservoirs. The side slopes changed between 30 to 90 degrees. The results showed that the lower side slopes create catastrophic outflows and the capacities and lengths of the reservoirs are two important parameters to peak discharge and time to outflow hydrograph peak. In addition, many studies have evaluated dam-break flow in the presence of obstacles with different shapes in downstream channel [21–25].

2. Innovation and studied reservoirs

Since in nature it is unlikely to find a dam reservoir with the exactly symmetric shape, in the present study, two real benchmarks are chosen, in contrast to the previous studies [15,16,20], which modeled some symmetric (and hypothetical) reservoirs. As it was reviewed, many attempts have been made to investigate different conditions of the dam-break phenomenon, but asymmetric shapes of real dams have never been examined. In fact, the sidewalls of the reservoir of each dam in reality have their own angles and it is not possible to examine all of them; hence, two prototypes were selected. Apart from two asymmetric reservoirs, two models with symmetric shapes (with 30 and 45 degrees), a model with 90-degree bend, and long reservoirs are simulated.

3. Methodology

Before beginning simulation according to proposed models, it is necessary to examine the accuracy of the numerical model using a laboratory model. For this purpose, the results of Martin and Moyce [26] and Abdolmaleki et al. [27] were used, which are the well-known studies in the dam-break studies. A horizontal rectangular glass flume with a length of 3.22 (m), width of 1 (m), and height of 2 (m) was used to conduct a laboratory experiment. The height and length of water in the reservoir were considered 0.6 and 1.2 (m), respectively. In these kinds of models when the model's gate is pulled up, the rectangular column of water in the reservoir is released at the instant of zero and goes towards downstream, according to the gravity force, and the waves are studied at different times. Various grid sizes and turbulence models are examined to obtain the most realistic results from the CFD solver. After model verification, six different reservoirs are used to evaluate dam-break flow considering reservoir shapes.

2.1. Numerical setup

FLOW-3D is one of the computational fluid dynamics (CFD) models, which is used in the present study to simulate dam-break flow, according to the different reservoirs geometries. Production and distribution of this model performed by Flow Science Inc. FLOW-3D model includes various physical models, including shallow water, turbulence, cavitation, viscosity, homogenous and adiabatic bubbles, porous media, sediment scour, surface tension, particles and also all types of heat transfer. Among all advantages of this model, also it is possible to add a DEM file in FLOW-3D to simulate flow over real topography, or to import a STL file from other software, such as AutoCAD. In FLOW-3D model, water is simulated by the volume of fluid (VOF) method, and Reynolds Averaged Navier Stokes (RANS) equations are solved with a

turbulence model. VOF method consists of three principal components, such as the definition of the volume of fluid function, setting the boundary conditions at the free surface, and a method to solve the VOF transport equation. Flow equations are solved numerically using finite-difference (or finite-volume) approximations. Flow region in FLOW-3D is subdivided into a mesh of fixed rectangular cells. Almost all terms in the equations are evaluated explicitly, but different implicit options also exist. The aforementioned approach provides a simple and efficient computational scheme for plenty of cases; however, it is necessary to use a limited time-step size to provide computationally stable and accurate results. There is an exception in this explicit formulation: By using time-advanced pressures, velocities and pressures are coupled implicitly in the momentum equations and time advanced velocities in the mass continuity equation. This semi-implicit method in the finite-difference equations allows for the efficient solution of low speed and incompressible flow problems. FLOW-3D has been used satisfactory in a range of studies in hydraulic engineering [28,29]. FLOW-3D version 11.0.4.03 is used in this study. Equations of fluid 3-D motion include mass continuity equation and momentum equations [30].

The general form of mass continuity equation in Cartesian coordinate is written as

$$V_F \frac{\partial \rho}{\partial t} + \frac{\partial}{\partial x}\left[\rho u A_x\right] + \frac{\partial}{\partial y}\left[\rho v A_y\right] + \frac{\partial}{\partial z}\left[\rho w A_z\right] = 0 \tag{1}$$

The motion equations for the three fluid velocity components (i.e., u, v, w) in the three coordinate directions are the Navier-Stokes equations, which are expressed as

$$\frac{\partial u}{\partial t} + \frac{1}{V_F}\left\{u A_x \frac{\partial u}{\partial x} + v A_y \frac{\partial u}{\partial y} + w A_z \frac{\partial u}{\partial z}\right\} = -\frac{1}{\rho}\frac{\partial p}{\partial x} + G_x + f_x \tag{2}$$

$$\frac{\partial v}{\partial t} + \frac{1}{V_F}\left\{u A_x \frac{\partial v}{\partial x} + v A_y \frac{\partial v}{\partial y} + w A_z \frac{\partial v}{\partial z}\right\} = -\frac{1}{\rho}\frac{\partial p}{\partial y} + G_y + f_y \tag{3}$$

$$\frac{\partial w}{\partial t} + \frac{1}{V_F}\left\{u A_x \frac{\partial w}{\partial x} + v A_y \frac{\partial w}{\partial y} + w A_z \frac{\partial w}{\partial z}\right\} = -\frac{1}{\rho}\frac{\partial p}{\partial z} + G_z + f_z \tag{4}$$

where VF = the fractional volume open to flow (-), ρ = fluid density (kg/m3), x, y, z = three-dimensional Cartesian coordinate system; u, v, w = velocity components (m/s) in x, y, z, directions, Ax, Ay, Az = the fractional area open to flow in x, y, z directions, p= pressure (Pa); G = body acceleration (m/s2); and f = viscous acceleration (m/s2). While G and f are of the acceleration type, the source of them is different. G can be produced by gravity or acceleration of the system or both. Viscous acceleration (f) involves the effects of molecular viscosity and viscosity due to turbulence, which is written as

$$f = \frac{1}{V_f}\left(\frac{\tau_{b,i}}{\rho} - \frac{\partial}{\partial x_i}\left(A_j S_{ij}\right)\right) \tag{5}$$

in which

$$S_{ij} = -\left(\nu + \nu_T\right)\left(\frac{\partial u_i}{\partial x_j} + \frac{\partial u_j}{\partial x_i}\right) \tag{6}$$

where $\tau_{b,i}$ = wall shear stress (Pa); S_{ij} = strain rate tensor; ν = kinematic viscosity (m^2/s); and ν_T = kinematic eddy viscosity (m^2/s).

On the other hand, in the current study, FLOW-3D performance is compared to that of FLUENT model, which is another widely-used CFD method. FLUENT is capable of simulating plenty of flow problems, including laminar, turbulent, incompressible and compressible fluids. To solve different problems, this model provides the volume of fluid (VOF), Eulerian models, mixture, and the discrete phase model, implementing Lagrangian trajectory calculations for dispersed phases (particles, droplets, or bubbles). In summary, FLUENT employs a broad range of mathematical models with the ability to model complex geometries, which has been acted successfully in many academic and industrial applications.

2.2. Simulation condition

To simulate experimental conditions in Flow-3D and verify the model performance, a channel with length, height, and width of 3.22, 2, and 1 (m) is created. The introduced fluid into the model is water with the temperature of 20 °C, viscosity coefficient of 0.001 (kg/m.s), and density of 1000 (kg/m3) which has a height of 0.6 (m) and a length equals to 1.2 (m). Gravity is defined with a magnitude of -9.81 (m/s^2). The reservoir and the channel are separated by a gate in the experimental model. In Fig. 1, the geometry of all six models (R1-R6) were shown. R6 is used for verifying the CFD model, too. Based on Fig. 1, all models have channels with a length of 2.02 (m), and width of 1 (m). Also, the bed of all models is horizontal and has identical water volume (i.e., 0.72 m3). In other words, all reservoirs have the same water volume and water height, but their geometries are different. In fact, model 1 (R1) belongs to Mahabad reservoir dam (Mahabad, Iran). The second model (R2) is a constructed concrete arch dam called Tignes dam, located in France. Aerial photos of these two case studies (Mahabad Dam and Tignes Dam) are shown in Fig. 2. R3 and R4 models have trapezoidal reservoirs with symmetrical sides with angles of 30 and 45 degrees, as shown in Fig. 1(c,d), respectively. R5 model is shown in Fig. 1(e), and has a rectangular shape extending from one side (bend). R6 model has a long and straight reservoir, as shown in Fig. 1(f). Five points are chosen to evaluate water height (h) and x-velocity (u) in the proposed models. The positions of these points (P1-P5) are shown in Fig. 1 and Table 1. In Table 1, the coordinate system (x, y) center (or 0, 0 point) is at the gate center. The studied reservoirs (including abutment, channel, and initial water) were created using AutoCAD 3D (v. 2016) and afterward were imported as STL files to FLOW-3D model. In Fig. 3, 3D views of these models (R1-R6) are shown.

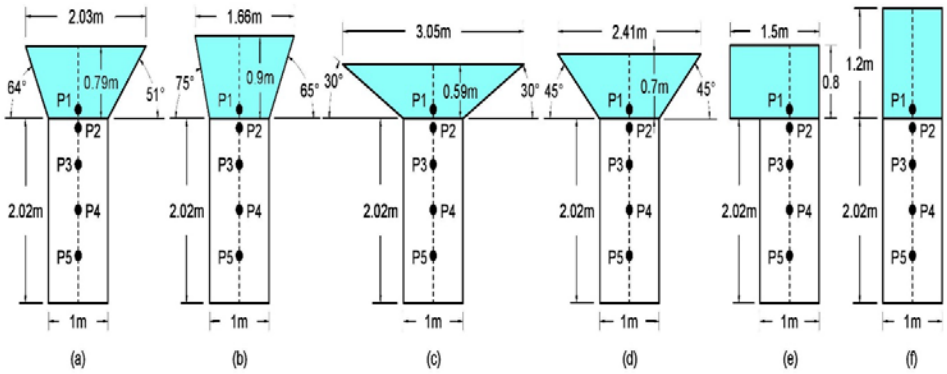

Fig. 1. Reservoir shapes: (a) R1 (Mahabad Dam), (b) R2 (Tignes Dam), (c) R3 (30 degree); (d) R4 (45 degree); (e) R5 (Bend); and (f) R6 (Long).

(a)

(b)

Fig. 2. Two case studies: (a) Mahabad Dam; (b) Tignes Dam.

Table 1
Positions of five points across the flume.

Point	*x* (m)	*y* (m)
P1	0	-0.10
P2	0	0.10
P3	0	0.50
P4	0	1.00
P5	0	1.50

2.3. Boundary condition

Figure 4 illustrates the boundary condition of the numerical model for verification. Boundary conditions should be set before beginning simulation to specify what happens at mesh edges. There are ten different boundary conditions in Flow-3D model: (1) symmetry; (2) continuative; (3) specified pressure; (4) grid overlay; (5) wave; (6) wall; (7) periodic; (8) specified velocity; (9) outflow; and (10) volume flow rate. In the current study, water cannot be added to the flume through inlet, escape from outlet and leak from channel bed. With this said, for the inlet and outlet boundaries of the computed region, a “wall” boundary condition is considered, which acts like a virtual wall. Also, the “wall” boundary condition is adopted at the bottom and two sides of the flume. The “symmetry” condition has some applications. For instance, this condition can be applied to the water free surface or also to models with more than one cubic mesh block. The outside and inside of this boundary condition is considered exactly the same and used for the top boundary of the model (Fig. 4).

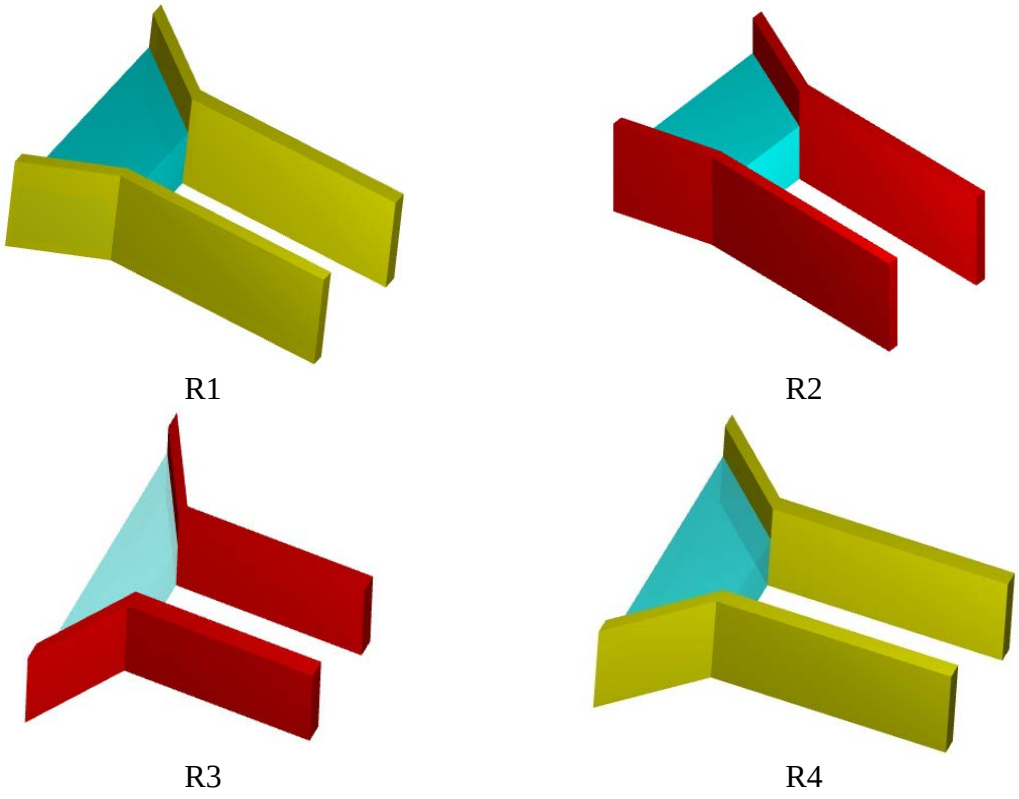

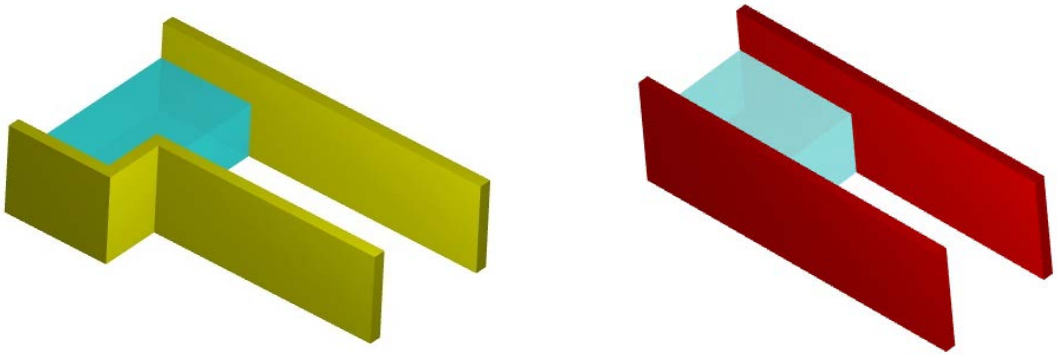

R5 R6

Fig. 3. Dam-break models for R1 (Mahabad Dam); R2 (Tignes Dam); R3 (30 degree); R4 (45 degree); R5 (Bend); and R6 (Long).

The current model will run for a period of time until the flow reaches and hits virtual wall at the end of flume. All the aforementioned information was employed to verify CFD model. In the proposed reservoirs (R1-R6), the same boundary conditions were used except the end of channel which ends with a free overflow condition, making water pass. Simulation time (t) is considered 5 (s).

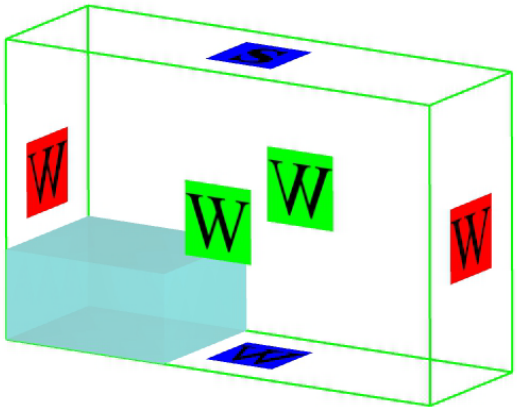

Fig. 4. Boundary conditions for dam-break model (in verification phase).

2.4. Turbulence model

As the stabilizing viscous forces are insufficient, the turbulence occurs, which is known as a chaotic and unstable motion of fluids. In situations with high values of Reynolds numbers, some natural instabilities happen in flow and the various sizes of eddies will be formed. Turbulence is observed in the most natural flows and it should be considered in all numerical models. The equations of mass and momentum conservation are used to simulate this behavior of flow. The resolution of mesh cells to simulate all details is important to meet desired results. Various turbulence models have been proposed. Some turbulence models are available in Flow-3D model, namely, Prandtl mixing length model, one-equation, two-equation standard k-ε and k-ω, renormalized group (RNG) k-ε model, and large eddy simulation (LES) model. The Prandtl mixing length model and one-equation model are the first attempts to represent turbulence. The Prandtl mixing length model is the least complex one and is used less and the one-equation

model is not recommended to simulate complex flows. The standard k-ε has been used successfully in a large variety of flows and the two-equation k-ω model is a good choice to model free shear flows such as spreading jets, wakes, and plumes. In the current study, k-ε, RNG, and k-ω turbulence models were used for the simulation of the unsteady flow caused by dam-break and the results were compared with the experimental data.

2.5. Resolution assessment criteria

Determination coefficient (R^2), root-mean-square error (RMSE), and mean absolute error (MAE) were used to assess resolutions. The equations are shown in Table 2.

Table 2
Equations of resolution assessment criteria.

Index	Symbol	Equation
Determination Coefficient	R^2	$1-\left[\sum_{i=1}^{N}(E-S)^2 / \sum_{i=1}^{N}E^2-\left(\sum_{i=1}^{N}S^2/N\right)\right]$
Root-Mean-Square Error	RMSE	$\left[\sum_{i=1}^{N}(E-S)^2/N\right]^{1/2}$
Mean Absolute Error	MAE	$\sum_{t=1}^{N}\lvert E-S\rvert/N$

Note: E = experimental value, S = simulated value, and N = number of data.

3. Results and discussion

Simulation using a CFD model is similar in many ways to that in laboratory. To simulate a real-life problem correctly, all details should be considered in both numerical and experimental models. By comparing numerical and experimental results using performance indices, one can guarantee the accuracy of the used model for incorporation of other changes to novelties. This stage in the simulation works is known as verification or validation.

3.1. Mesh resolution assessing

Choosing an appropriate size of the computational mesh is one of the most significant parts of the simulation setup. The suitable number or size of the mesh cells is essential to resolve the model geometry and flow features. By selecting the mesh sizes too coarse, all parts of the geometry of model may not be resolved and the actual problem may not be represented; conversely, by choosing them too fine, the computational time may increase unnecessarily. In the present research, four mesh sizes (i.e., 10, 20, 30, and 50 (mm) of each side) were examined to determine the highest simulation accuracy using three performance assessment criteria and the least time. The water level (m) data is used to calculate three performance indices. The results of the assessment of each mesh size and the computational time are shown in Table 3. The mesh cells with dimensions of 30×30×30 (mm) were chosen because it had the least value of RMSE and MAE indices and the highest value of R2 in comparison to other mesh cells. The computational time is also reasonable in comparison to 10 (mm) meshes which need more than five hours to simulate.

3.2. Turbulence models resolution assessing

Table 4 shows the results of three turbulence models, which were used to compare Flow-3D resolution with the experimental data to simulate dam-break flow. According to the three performance assessment indices, the k-ε model performed better, which also has been used in many previous dam-break studies for rapidly varied unsteady flows of high Reynolds numbers [17,31–35]. k-ε [36] is a semi-empirical model which calculates k and ε (turbulence kinetic energy and dissipation rate) [34] and finds LT (i.e., turbulence mixing length). In addition, the performance of the three turbulence models to simulate water level is shown in Fig. 5. Based on Fig. 5, all three models succeeded in simulating flow condition, but k-ε model was more successful to simulate peak water level at approximately $\tau = 7$ (τ = non-dimensionalised time).

Table 3
Mesh sizes assessment.

Index	Mesh Size (mm)			
	10×10×10	**20×20×20**	**30×30×30**	**50×50×50**
R^2 (%)	83.7	85.7	92.4	86.4
RMSE (m)	0.098	0.102	0.086	0.105
MAE (m)	0.087	0.087	0.078	0.093
Computational time (s)	19026	1034	217	33

Table 4
Turbulence models assessment.

Index	**Turbulence Model**		
	k-ε	**RNG**	**k-ω**
R^2 (%)	92.4	89.5	90.3
RMSE (m)	0.086	0.093	0.091
MAE (m)	0.078	0.085	0.082
Computational time (s)	217	174	237

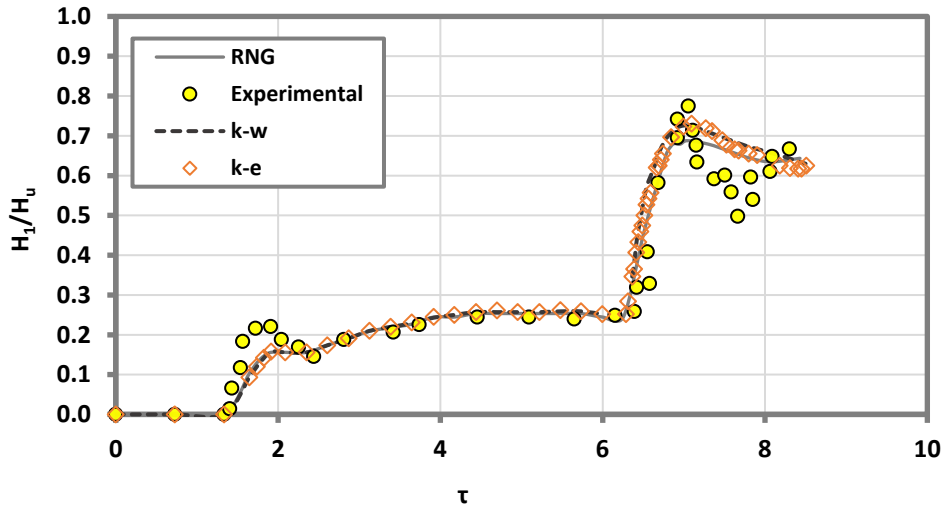

Fig. 5. Comparison of three turbulence models performance to simulate water level at 2.228 (m).

3.3. FLOW-3D and FLUENT models resolution assessing

To validate FLOW-3D, the comparison of the water height ratio in the two selected positions (i.e., at 2.228 and 2.725 (m) from the left-hand side of flume) are shown in Figs. 6 and 7, respectively, with the experimental results. In most parts of Figs. 6 and 7, the water heights which are calculated using two numerical models were at the same levels and their trends were well-modeled. As it is obvious, both models were unsuccessful to simulate the water levels caused by unsteady flow of the broken dam at the last time steps. These errors may have been produced due to the imperfect initial conditions and lack of simulation of all physical conditions of the actual sample, including channel friction, the dependence of these software on the turbulence models and the number and shape of the meshes.

As can be seen in Figs. 6 and 7, it can be concluded that the results of the FLOW-3D model are similar to the experimental results in comparison with the FLUENT (at all time steps). The resolution of the numerical models was shown in Table 5 using three performance indices. Results proved that FLOW-3D had superior performance in dam-break simulation in comparison to FLUENT.

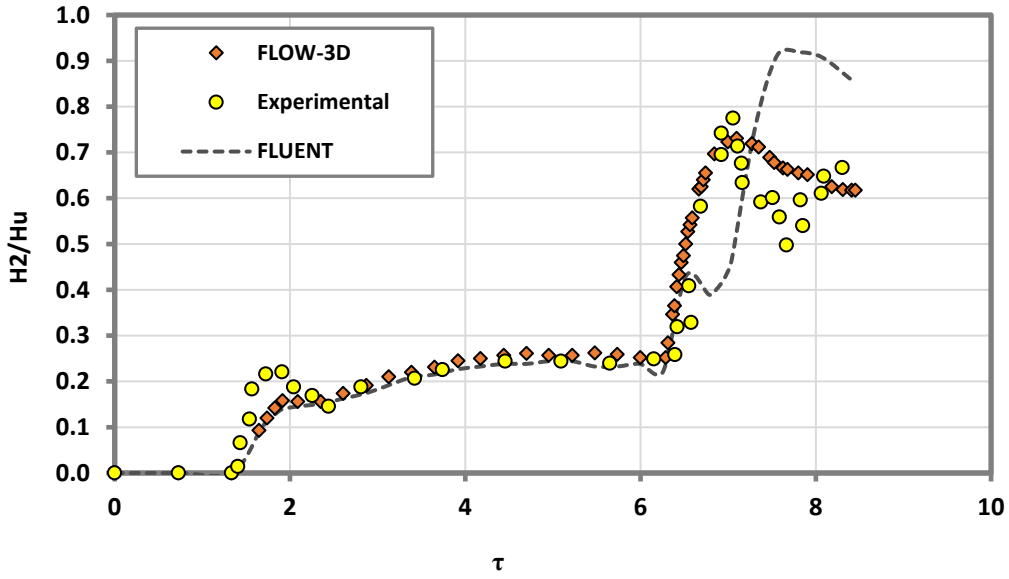

Fig. 6. Comparison of water level at 2.228 (m) using numerical models and experimental data.

Table 5
Comparison of the numerical models and experimental data.

Index	FLOW-3D	FLUENT
R^2 (%)	92.4	0.711
RMSE (m)	0.086	0.324
MAE (m)	0.078	0.211

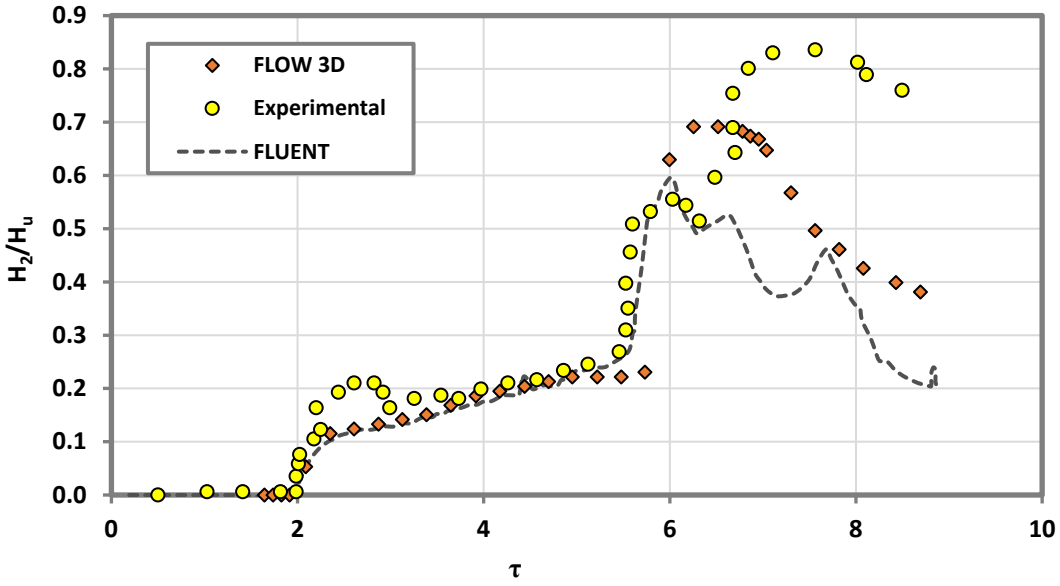

Fig. 7. Comparison of water level at 2.725 (m) using numerical models and experimental data.

Note: H1 and H2 are water levels at distance of 2.228 and 2.725 (m) from the beginning point of flume, respectively, Hu is initial water height, and τ is non-dimensionalised time (τ = t×(g/Hu)1/2).

In Fig. 8, flow conditions in a flume were shown for a better comparison of FLOW-3D and FLUENT simulations at different times. It is worth mentioning that different mesh sizes were employed to dam-break flow using FLUENT, such as 10, 30, 50, and 100 (mm), but the best result was obtained when meshes with dimensions of 30 and 15 (mm) were used [27]. In addition, it was mentioned that results were more sensitive to the sizes of meshes rather than time step and also using finer meshes beyond a specific level cannot enhance the free-surface resolution. As results for viscous and inviscid were similar, Abdolmaleki et al. [27] stated that water viscosity is not important for the dam-break problem. While k-ε model was used in Abdolmaleki et al. [27], it caused an artificial viscosity. It can be concluded that FLOW-3D could simulate dam-break flow with more coarse meshes and probably less computational time and better resolution, as well.

3.4. Water level analysis

Figure 9(a–e) compares water level variations at the aforementioned points (P1-P5) – one point at the upstream (inside the reservoirs) and four points at the downstream (along the channels). The initial water level was 0.6 (m) for all six models. Tables 6 and 7 summarize the peak water level and its arrival time for six reservoirs (R1-R6) at 5 points (P1-P5). No specific variation can be seen in Fig. 9(a), which shows water level variations at the point inside the reservoir (P1), except a small increase at the water level of R5 model before t=2 (s).

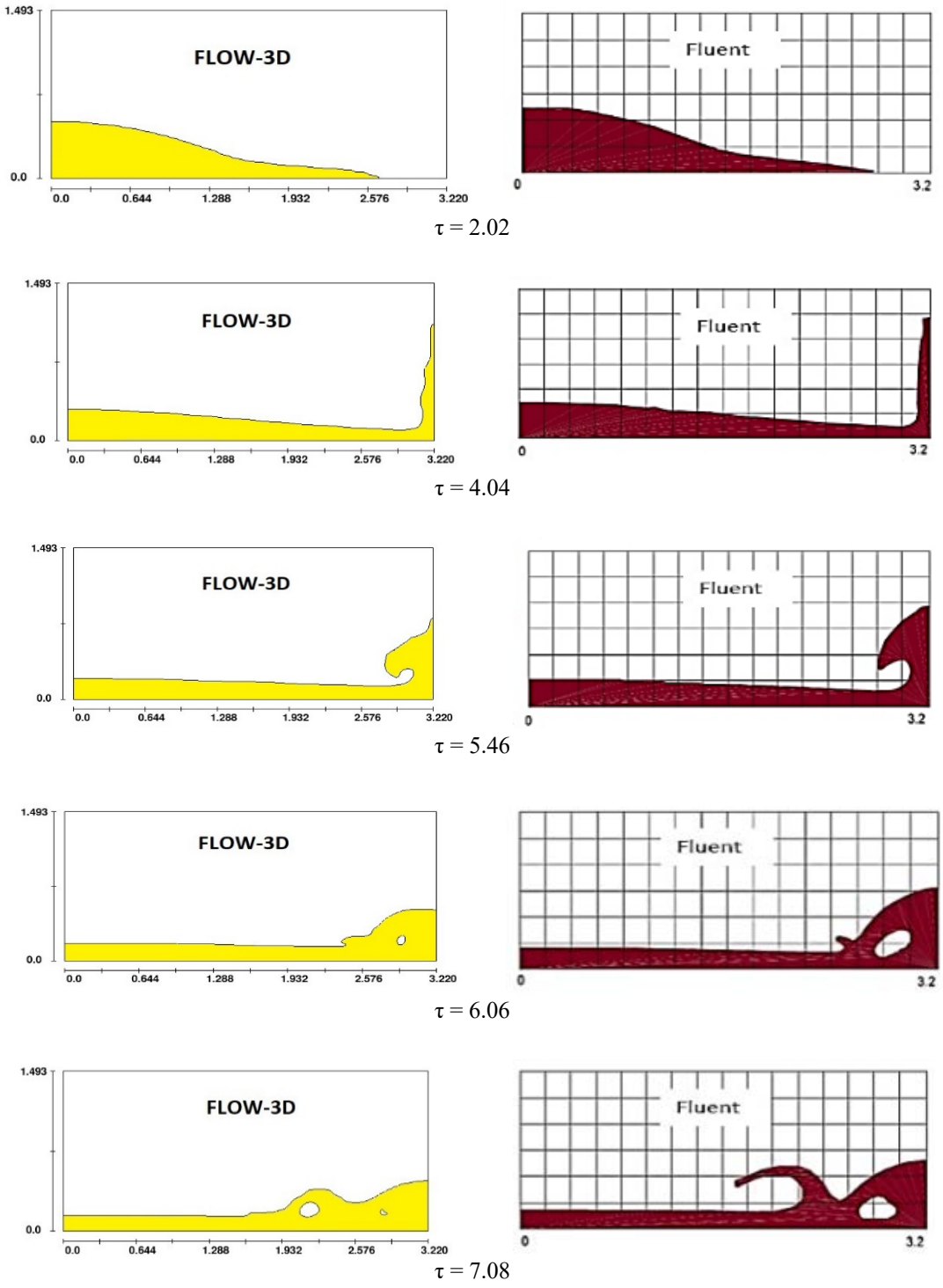

Fig. 8. Comparison of flow simulation using FLOW-3D and FLUENT models at different time steps.

Data in Fig. 9(b) were extracted from point P2, which is placed at 0.1 (m) downstream of the gate. Figure 9(b) shows that R3 model (symmetric reservoir with 30°) presents the highest water level, with 0.3289 (m) height at t= 0.2507 (s), based on Tables 6 and 7. According to Fig. 1, R3

has the shortest reservoir length. In Fig. 9(b), a similar trend is seen for all reservoirs after t = 2 (s). Figure 9(c) compares water level at point P3, which has a 0.5 (m) distance from the gate. It is noticeable that the highest measured water level at P3 belonged to R4, with 0.2296 (m) at t= 0.7982 (s). On the other hand, water level for R6 experienced the lowest value at about t= 1 (s), with 0.1879 (m) height. R1 and R2 had a similar trend at P3 during the computational time. In Fig. 9(d) water levels at P4 are shown. According to this Figure, after t= 3 (s) water levels follow the same trend. Water level for R4 hits the peak with 0.1536 (m) at 0.7982 (s) (Tables 6 and 7). The second highest water level belongs to R6 with a little difference (Table 6) and the lowest peak is for R5. Peak water level for R5 marked approximately the same trend in Fig. 9(d,e) – it had an increase before t= 3 (s). Peak water level at P5 reached 0.14 (m), at its highest value, for R4 after 1.8476 (s), based on Fig. 9(e). After t= 3 (s), water levels for all models followed the same trend.

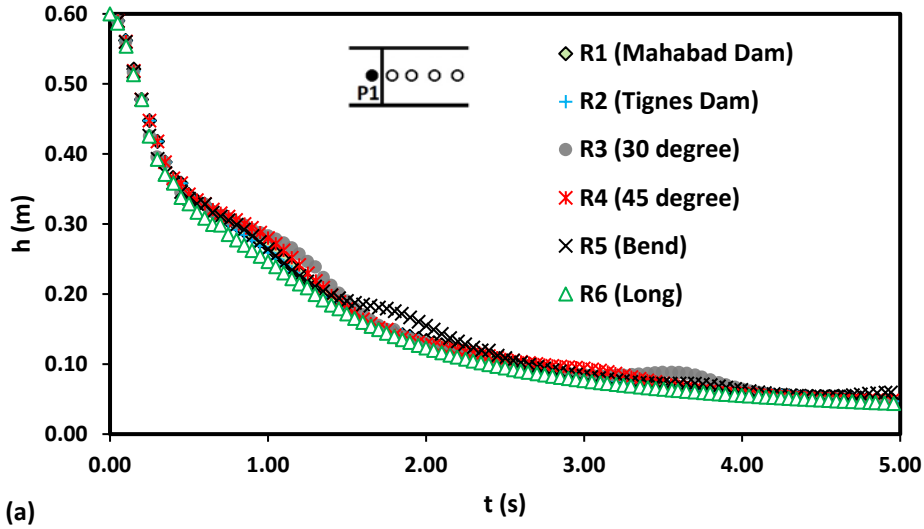

(a)

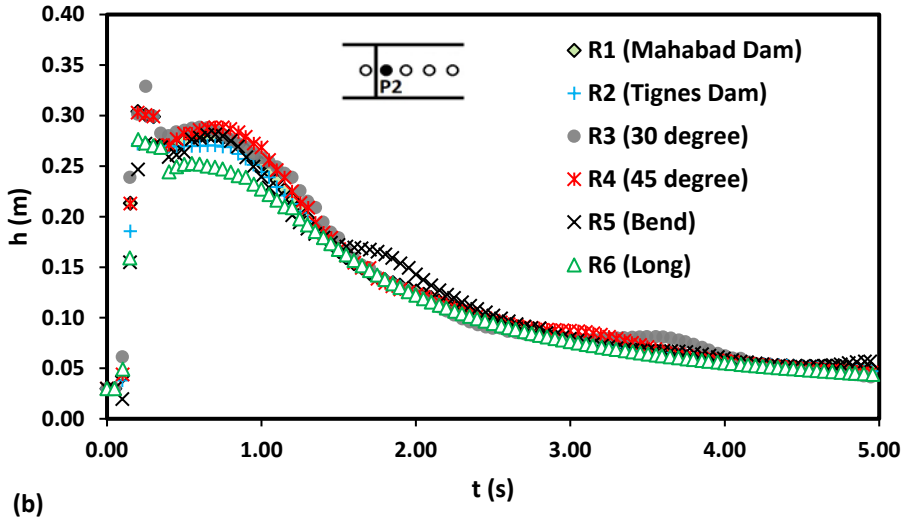

(b)

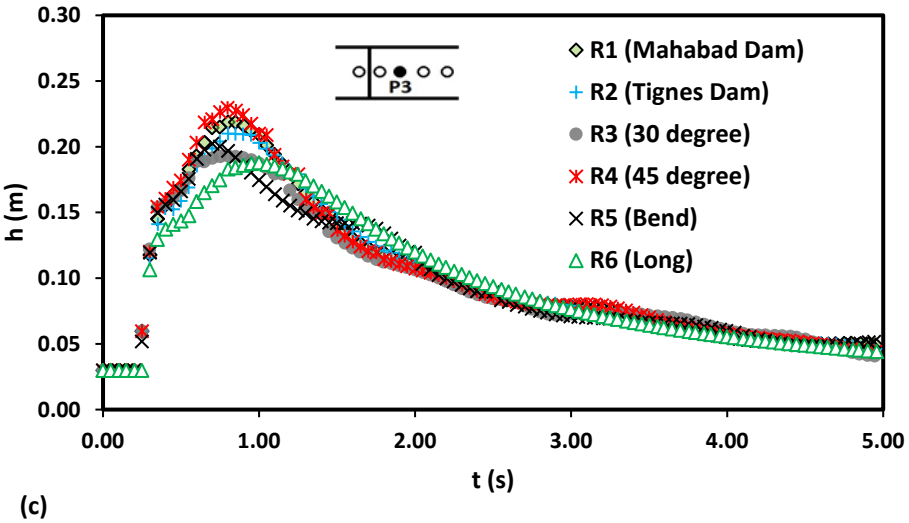

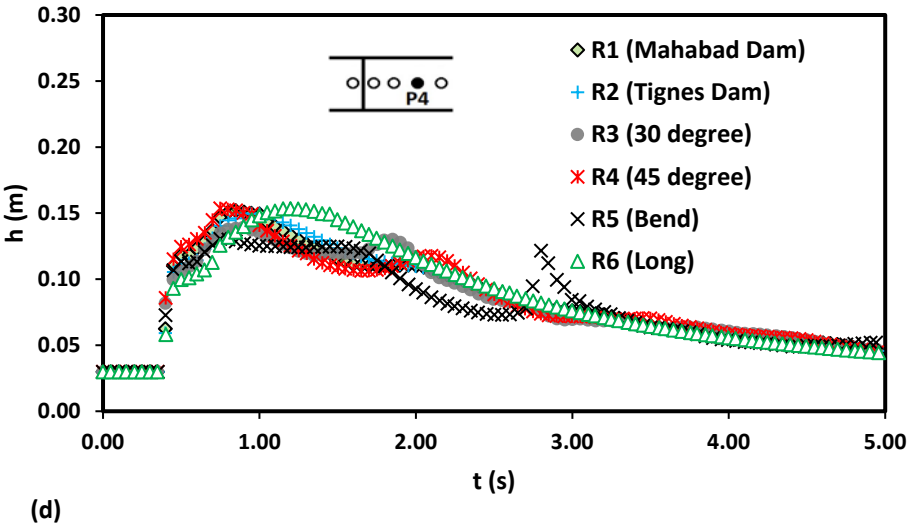

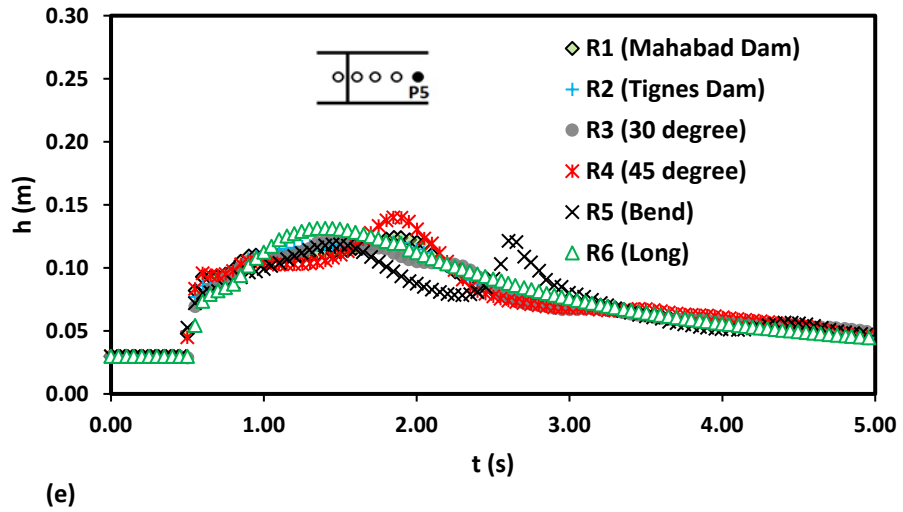

Fig. 9. Water levels at five points (i.e., P1-P5).

Table 6
Peak water levels.

Point	Peak Water Level in Reservoirs (m)					
	R1	**R2**	**R3**	**R4**	**R5**	**R6**
P1	0.6	0.6	0.6	0.6	0.6	0.6
P2	0.3040	0.3003	0.3289	0.3029	0.2815	0.2764
P3	0.2187	0.2100	0.1932	0.2296	0.2024	0.1879
P4	0.1518	0.1497	0.1391	0.1536	0.1304	0.1533
P5	0.1241	0.1208	0.1239	0.1400	0.1214	0.1314

Table 7
Arrival times for peak water levels.

Point	Peak Water Level Arrival Time in Reservoirs (s)					
	R1	**R2**	**R3**	**R4**	**R5**	**R6**
P1	0	0	0	0	0	0
P2	0.1993	0.2506	0.2507	0.1984	0.2489	0.2014
P3	0.8013	0.8019	0.7992	0.7982	0.7013	0.9998
P4	0.8485	0.9489	0.8985	0.7499	0.7497	1.1991
P5	1.8520	1.8005	1.4484	1.8476	2.6012	1.4010

Based on Table 6, peak water level for R4 reservoir had the highest value at three points i.e., P3-P5, because of its reservoir shape – R4 has the second shortest reservoir. On the other hand, R6 had two lowest peaks, at points P2 and P3 (i.e., at the beginning of the downstream channel), because it has the longest reservoir. Among the six models, R1 and R2 had approximately the same trends and peak water levels.

R3 had the highest peak value among all models, with 0.3289 (m). This reservoir also had two other unique characteristics among all models: the widest and shortest reservoir shape, with 3.05 (m) and 0.59 (m), respectively (Fig. 1). Accordingly, R4 which had the highest peak at three points, had the second widest and shortest reservoir shape, after R3 model. Apart from the two aforementioned models, about one third of water volume for R5 was stored behind the reservoir wall, which may cause variations after a short time after dam-break.

In addition, in Fig. 10, the free surface elevation for all reservoirs at t= 0.25, 0.5, 1 and 2 (s) is shown.

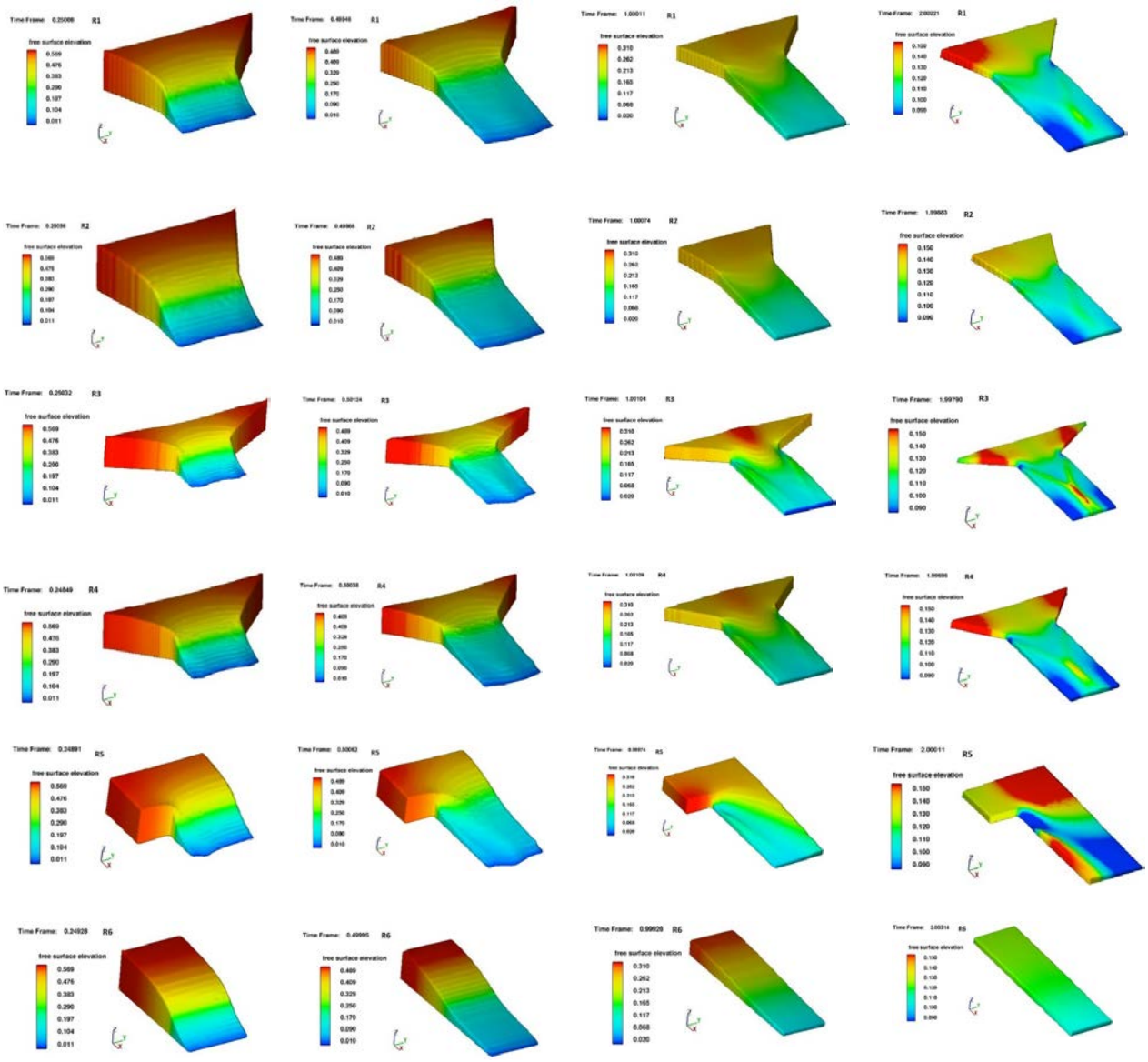

Fig. 10. Free surface elevation for all reservoirs at t= 0.25, 0.5, 1, and 2 (s).

3.5. Velocity analysis

Figure 11(a-e) shows the velocity component in x direction [u (m/s)] variations at channel bed relative to the time variations [t (s)] at five points (i.e., P1-P5). The starting point at the horizontal axis represents the moment when the column of water is released. Based on Table 8, the highest recorded velocity belonged to R6 (long reservoir) with 1.3073 (m/s) at P1. According to Fig. 11(a) and Tables 8 and 9, R1-R5 models hit the peak approximately before t= 0.2 (s), but R6 hit the peak just after t= 0.74 (s). The lowest peak velocity among six models at P1 point belonged to R4, with 1.1905 (m/s). Although all models have slightly the same trend at P1, R6 (long reservoir) had higher velocities at around t= 0.7 (s). In fact, R6 represented a straight weir constructed in a rectangular channel, rather than showing the status of a broken dam. Figure

11(b) shows that the highest velocity at P2, which has a 0.10 (m) distance from the gate (in other words, a broken dam), belonged to R5. The flow velocity was almost equal at points P3-P5,and there is no significant variation except a small increase for R5 before t= 3 (s).

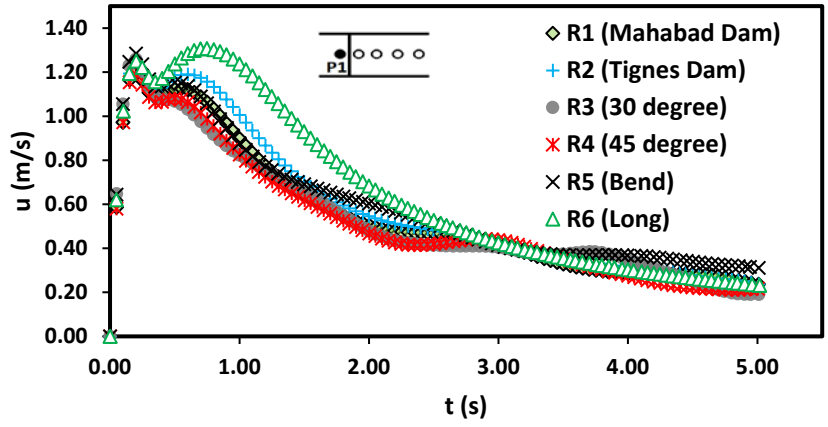

(a)

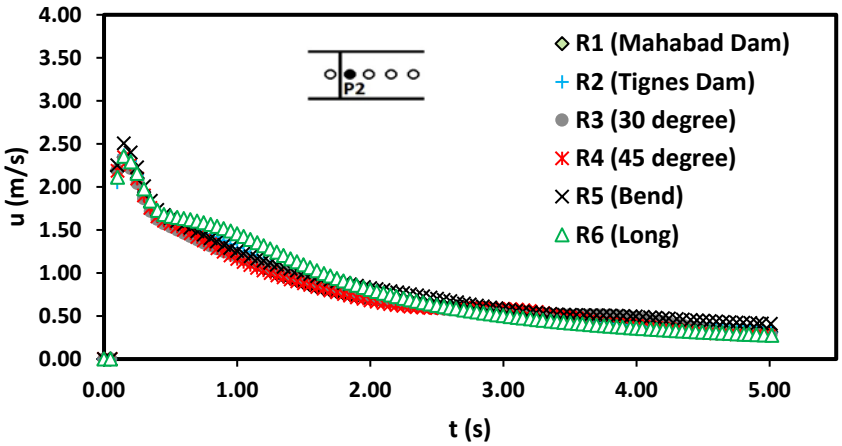

(b)

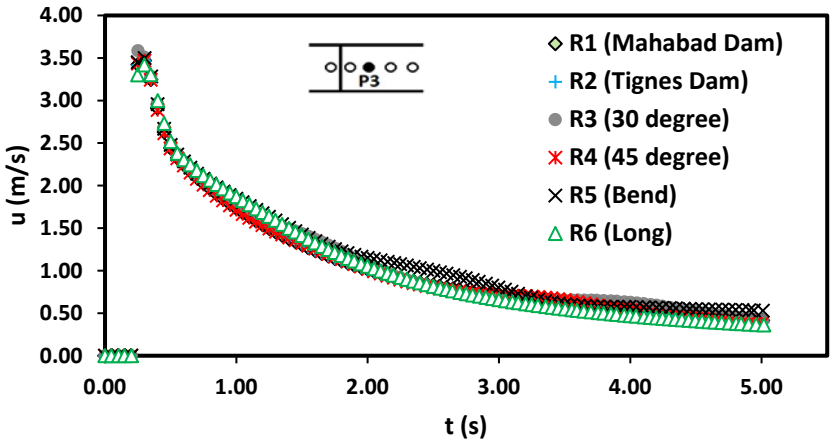

(c)

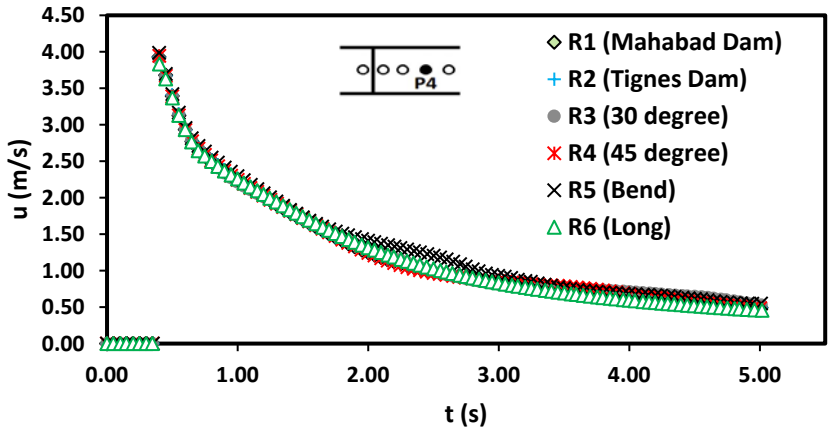

(d)

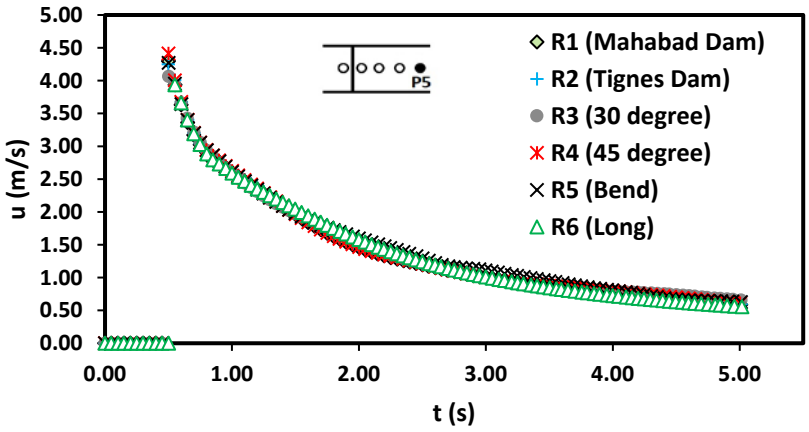

(e

Fig. 11. Velocity component in x direction at five points (P1-P5).

Table 8
Peak velocity component in *x* direction (*u*).

Point	Peak *x*-velocity in Reservoirs (m/s)					
	R1	R2	R3	R4	R5	R6
P1	1.2046	1.2410	1.2594	1.1905	1.2850	1.3073
P2	2.3451	2.3702	2.3339	2.3453	2.5066	2.3559
P3	3.4689	3.4654	3.5849	3.4678	3.4990	3.4185
P4	3.9304	3.9293	3.9022	3.9448	3.9856	3.8332
P5	4.2957	4.2482	4.0636	4.4151	4.2694	3.9359

Table 9
Time of peak velocity component in *x* direction.

Point	Peak *x*-velocity Time in Reservoirs (s)					
	R1	R2	R3	R4	R5	R6
P1	0.1993	0.1986	0.1993	0.1984	0.2005	0.7485
P2	0.1506	0.1507	0.1484	0.1510	0.1487	0.1483
P3	0.3010	0.2987	0.2507	0.3005	0.3012	0.2998
P4	0.3987	0.3985	0.3989	0.4007	0.4000	0.4016
P5	0.4995	0.4987	0.5013	0.4995	0.5006	0.5504

The lowest peak velocity value among the six models was for R4 model, which is asymmetric reservoir. At P3 point, R3 had the highest velocity in x direction, with 3.5849 (m/s). It is noticeable that there are no significant differences at P4 and P5 points and almost all reservoirs had a similar trend. R4 at P5 had a little greater velocity value compared to other reservoirs (Table 8).

While R6 had the highest velocity at P1 (the point inside of reservoir), it had the lowest velocity at three points (P3-P5), which are situated at the end of reservoir. On the other hand, R5 had two highest peak velocities at P2 and P4. In addition, in Fig. 12, the velocity component in x direction for all reservoirs at t= 0.25, 0.5, 1 and 2 (s) are shown.

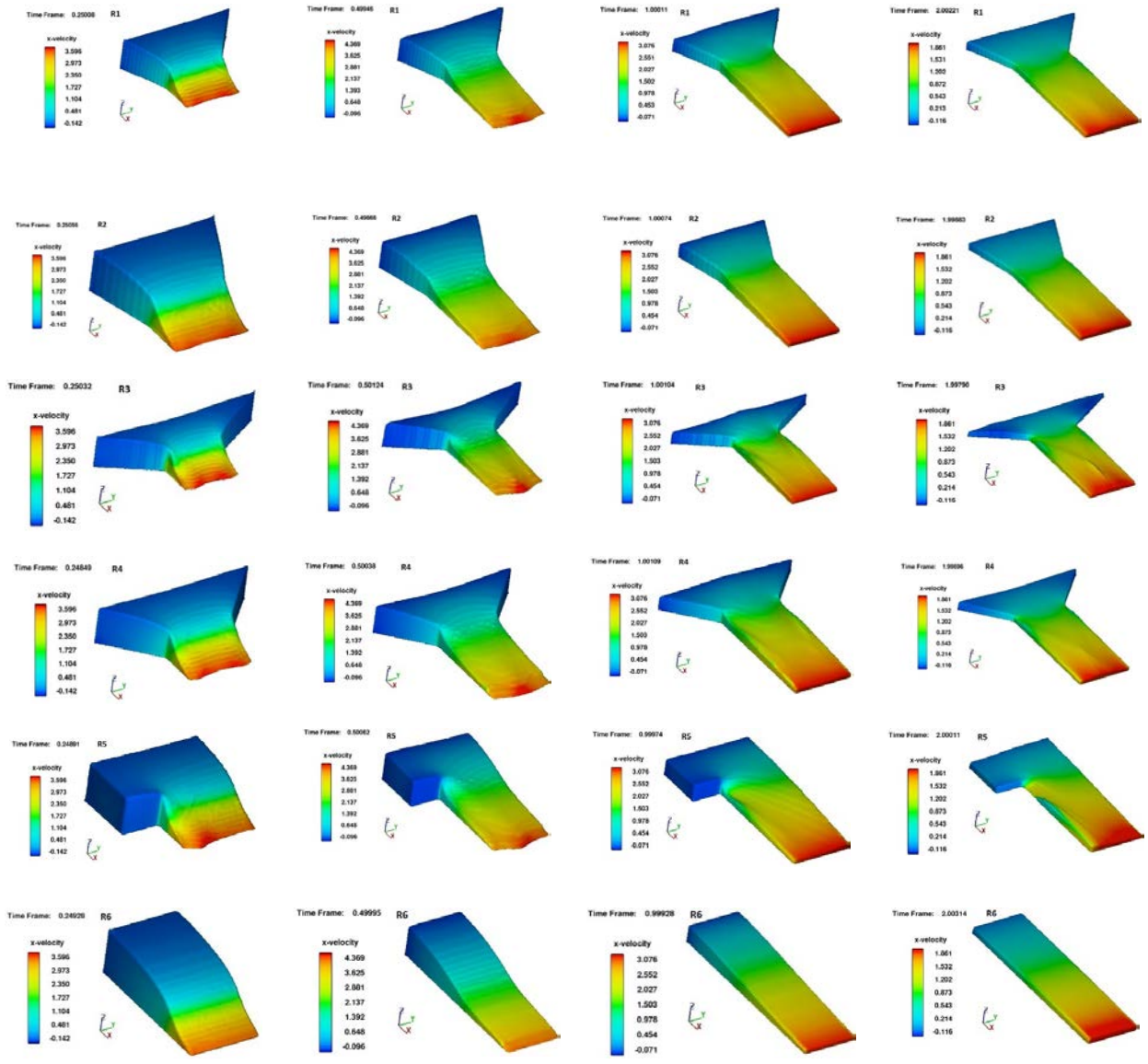

Fig. 12. *x*-velocity for all reservoirs at t= 0.25, 0.5, 1, and 2 (s).

3.6. Water surface profiles analysis

In Fig. 13, water surface profiles of all models (R1-R6) are shown. Also, the positions of gates (G1-G6) are shown. Based on Fig. 1, the downstream channels for all models are of the same length (i.e., 2.02 (m)), but the length of reservoirs is different. The longest reservoir is for R6 and the shortest is for R3. Figure 13(a), compares water surface profiles at t= 1 (s). In Fig. 13(a), models R1-R5 had approximately the same trend, except R3 that had more value before x= 0.5 (m). At t= 2 (s) i.e., Fig. 13(b), R5 had more water levels before gate, but it reduced along the upstream channel and reached the lowest value at the end of the channel.

Water levels for R3 saw an increase at approximately x= 2 (m) and t= 2 (s), which can be seen in Fig. 10, too. R1, R2, and R4 also followed this trend, but their value was less than R3 (Fig. 10). It is noticeable that R6 (long reservoir) water profiles had a constant steep at all time frames. In Fig. 13(c-e), all reservoirs had almost the same trend except R5, which had an increase after x= 1.5 (m).

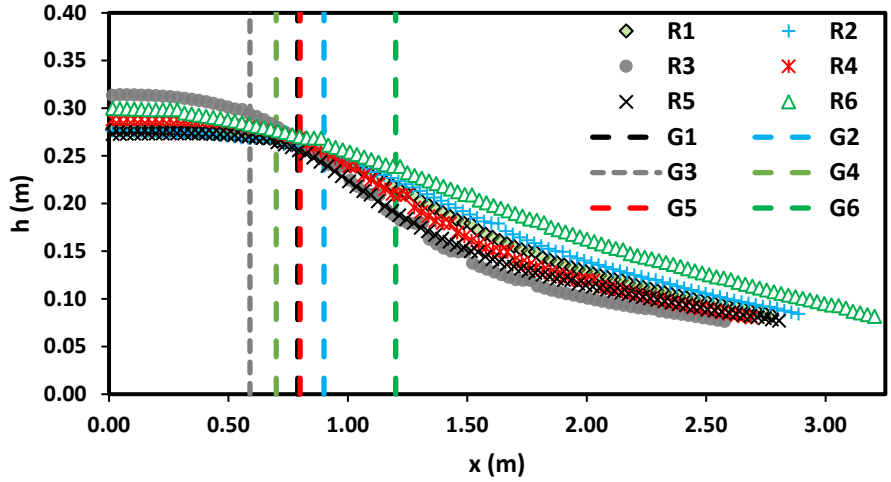

(a)

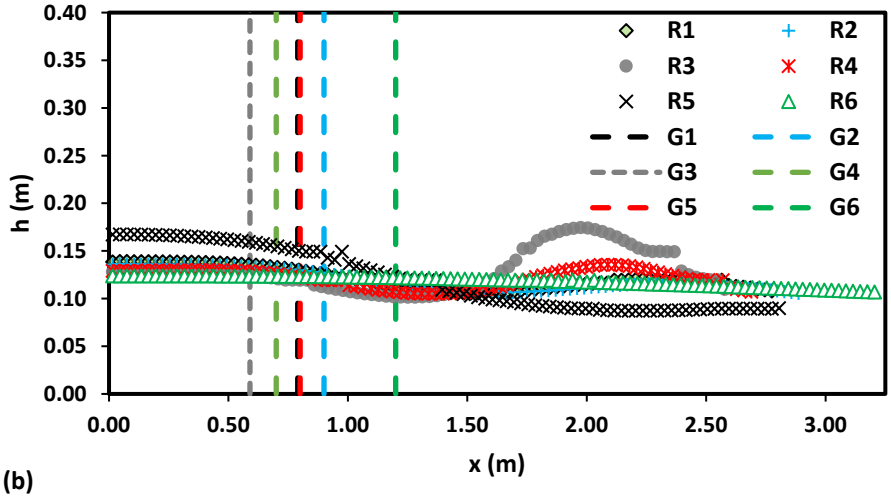

(b)

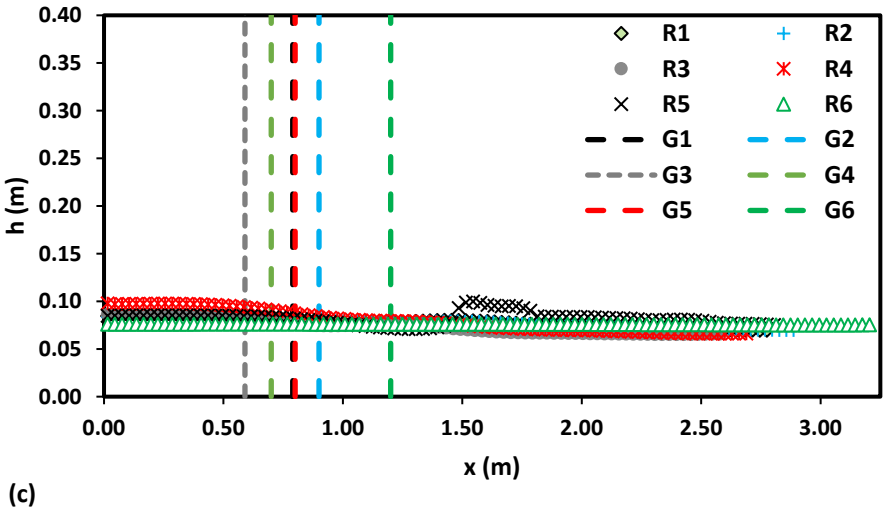

(c)

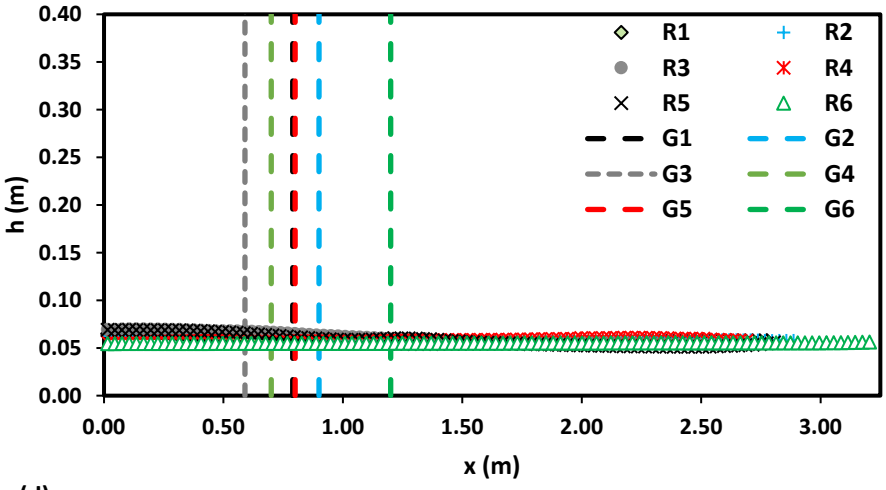

(d)

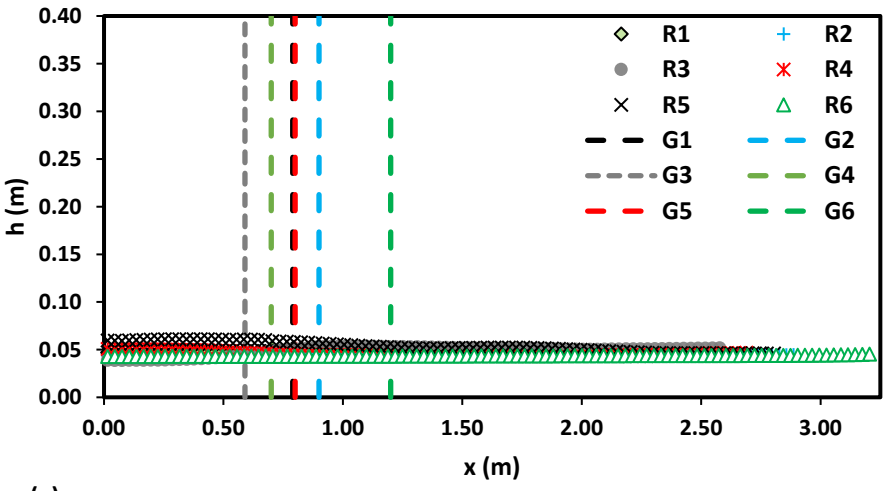

(e)

Fig. 13. Water surface profiles (h) along flume length at (a) t = 1 (s), (b) t = 2 (s), (c) t = 3 (s), (d) t = 4 (s) and (e) t = 5 (s).

Note: G1-G6 are positions of gates for R1-R6 reservoirs.

4. Conclusions

In the present study, the unsteady flow caused by dam-break was studied. Simulation was performed using the FLOW-3D model and results were compared to a laboratory study and a FLUENT model. The results of the sensitivity analysis with the laboratory model showed that the k-ε turbulence model was the most suitable choice. Also, to select the size of the meshes, after examining several cell sizes, cubic cells with 30 (mm) dimensions were selected.

The results have been analyzed at the two selected sections along the channel, it can be concluded from the results of these two models and the laboratory study in which both models had satisfactory capabilities in modeling unsteady flow, but they also had some weaknesses, which might be due to the imperfect initial conditions and lack of simulation of all physical conditions of the actual sample, including channel friction, the dependence of these software on the turbulence models and the number and shape of the meshes. According to the performance criteria (R2, RMSE, MAE), it can be concluded that the FLOW-3D model was more capable than FLUENT to simulate experimental condition of this problem.

Since the main objective of this study was to investigate the effect of different reservoir shapes on dam-break flow, six different models were investigated. As real dams have not symmetric reservoir geometries, in the current study, instead of symmetric reservoirs which have been evaluated in the previous researches, two models were selected based on real dams, with asymmetric reservoirs. This numerical study is based on the fact that there is no proposed solution to this problem. Considering the present results of flow velocities and height of dam-break flow, it can be proved that dam-break flow varies from one dam to another, considering reservoir geometry. The most important features of the reservoirs studied are as follows: (1) Water level and velocity in R1 and R2 models (asymmetric reservoirs) did not have any special features and had almost the same trend; (2) Among all models, R3 (symmetric reservoir with 30°), which had the widest and shortest reservoir shape, had the highest peak water level; (3) R4 (symmetric reservoir with 45°) had the highest peak water level at three points at the end of downstream channel (i.e., P3-P5); (4) The highest measured velocity in x direction belonged to R4; (5) The water level in R5, which represented a reservoir with a bend, had a different trend at the end of channel, this may have occurred because approximately one third of water volume was stored behind the reservoir wall; (6) The longest reservoir (R6) had the highest velocity at the first point (P1). In general, this study was conducted in a relatively small channel, suggesting that larger flumes may be used in future studies.

Funding
This research received no external funding.

Conflicts of Interest
The authors declare no conflict of interest.

Authors Contribution Statement
Ahmad Ferdowsi: Conceptualization; Formal analysis; Investigation; Methodology; Software; Validation; Validation; Visualization; Writing – original draft; Writing – review & editing.

Mahmood Nemati: Conceptualization; Formal analysis; Investigation; Methodology; Software; Validation. Saeed Farzin: Conceptualization; Methodology; Validation; Writing – review & editing; Supervision.

References

[1] Kojima H, Kohgo Y, Shimada K, Shoda D, Suzuki H, Saito H. Numerical modeling of flood flow after small earthen dam failure: a case study from the 2011 Tohoku earthquake. Paddy Water Environ 2020;18:431–42. doi:10.1007/s10333-020-00792-w.

[2] Chen S-H. Hydraulic Structures. Berlin, Heidelberg: Springer Berlin Heidelberg; 2015. doi:10.1007/978-3-662-47331-3.

[3] Larocque LA, Imran J, Chaudhry MH. 3D numerical simulation of partial breach dam-break flow using the LES and k –ϵ turbulence models. J Hydraul Res 2013;51:145–57. doi:10.1080/00221686.2012.734862.

[4] Sangsefidi Y, Mehraein M, Ghodsian M. Experimental study on flow over in-reservoir arced labyrinth weirs. Flow Meas Instrum 2018;59:215–24. doi:10.1016/j.flowmeasinst.2017.12.002.

[5] Safarrazavi Zadeh M, Esmaeili Varaki M, Biabani R. Experimental study on flow over sinusoidal and semicircular labyrinth weirs. ISH J Hydraul Eng 2019:1–10. doi:10.1080/09715010.2019.1644679.

[6] Nayyer S, Farzin S, Karami H, Rostami M. A numerical and experimental investigation of the effects of combination of spur dikes in series on a flow field. J Brazilian Soc Mech Sci Eng 2019;41:256. doi:10.1007/s40430-019-1757-0.

[7] Ferdowsi A, Farzin S, Mousavi S-F, Karami H. Hybrid Bat & Particle Swarm Algorithm for optimization of labyrinth spillway based on half & quarter round crest shapes. Flow Meas Instrum 2019;66:209–17. doi:10.1016/j.flowmeasinst.2019.03.003.

[8] Ferdowsi A, Hoseini SM, Farzin S, Faramarzpour M, Mousavi S-F. Shape optimization of gravity dams using a nature-inspired approach. J Soft Comput Civ Eng 2020;4:65–78.

[9] Ferdowsi A, Valikhan-Anaraki M, Mousavi S-F, Farzin S, Mirjalili S. Developing a model for multi-objective optimization of open channels and labyrinth weirs: Theory and application in Isfahan Irrigation Networks. Flow Meas Instrum 2021;80:101971. doi:10.1016/j.flowmeasinst.2021.101971.

[10] Ferdowsi A, Singh VP, Ehteram M, Mirjalili S. Multi-objective Optimization Approaches for Design, Planning, and Management of Water Resource Systems, 2021, p. 275–303. doi:10.1007/978-981-33-4295-8_11.

[11] Ferdowsi A, Mousavi S-F, Farzin S, Karami H. Optimization of dam's spillway design under climate change conditions. J Hydroinformatics 2020;22:916–36. doi:10.2166/hydro.2020.019.

[12] Bell SW, Elliot RC, Hanif Chaudhry M. Experimental results of two-dimensional dam-break flows. J Hydraul Res 1992;30:225–52. doi:10.1080/00221689209498936.

[13] STANSBY PK, CHEGINI A, BARNES TCD. The initial stages of dam-break flow. J Fluid Mech 1998;374:407–24. doi:10.1017/S0022112098001918.

[14] Xue Y, Xu W, Luo S, Chen H, Li N, Xu L. Experimental Study of Dam-Break Flow in Cascade Reservoirs With Steep Bottom Slope. J Hydrodyn 2011;23:491–7. doi:10.1016/S1001-6058(10)60140-0.

[15] Feizi Khankandi A, Tahershamsi A, Soares-Frazão S. Experimental investigation of reservoir geometry effect on dam-break flow. J Hydraul Res 2012;50:376–87. doi:10.1080/00221686.2012.690974.

[16] Farzin S, Alizadeh M, Hassanzadeh Y. Numerical Simulation of Unsteady One-Dimensional Dam-

Break Flows Using TVD MacCormack Scheme n.d.

[17] Farzin S, Hassanzadeh Y, Aalami MT, Fatehi R. Analysis of Dam Break Problem Using a Lagrangian Method and Comparing it with Eulerian Approach. Iran-Water Resour Res 2014;10:87–105.

[18] Farzin S, Hassanzadeh Y, Alami MT, Fatehi R. An implicit incompressible SPH method for free surface flow problems. Modares Mech Eng 2014;14:99–110.

[19] Wood A, Wang K-H. Modeling dam-break flows in channels with 90 degree bend using an alternating-direction implicit based curvilinear hydrodynamic solver. Comput Fluids 2015;114:254–64. doi:10.1016/j.compfluid.2015.03.011.

[20] Hooshyaripor F, Tahershamsi A, Razi S. Dam break flood wave under different reservoir's capacities and lengths. Sādhanā 2017;42:1557–69. doi:10.1007/s12046-017-0693-x.

[21] Kocaman S, Ozmen-Cagatay H. The effect of lateral channel contraction on dam break flows: Laboratory experiment. J Hydrol 2012;432–433:145–53. doi:10.1016/j.jhydrol.2012.02.035.

[22] Marsooli R, Wu W. 3-D finite-volume model of dam-break flow over uneven beds based on VOF method. Adv Water Resour 2014;70:104–17. doi:10.1016/j.advwatres.2014.04.020.

[23] Issakhov A, Zhandaulet Y, Nogaeva A. Numerical simulation of dam break flow for various forms of the obstacle by VOF method. Int J Multiph Flow 2018;109:191–206. doi:10.1016/j.ijmultiphaseflow.2018.08.003.

[24] Kurokawa FA, Corrêa L, Queiroz RAB de. Numerical simulation of 3D unsteady turbulent free surface flows using $$\kappa -\varepsilon$$ κ - ε model and ADBQUICKEST scheme. J Brazilian Soc Mech Sci Eng 2018;40:202. doi:10.1007/s40430-018-1100-1.

[25] Issakhov A, Imanberdiyeva M. Numerical simulation of the movement of water surface of dam break flow by VOF methods for various obstacles. Int J Heat Mass Transf 2019;136:1030–51. doi:10.1016/j.ijheatmasstransfer.2019.03.034.

[26] Moyce WJ, Martin JC. An experimental study of the collapse of liquid columns on a rigid horizonal plane. Philos Trans Roy Soc London A 1952;244:312–24.

[27] Abdolmaleki K, Thiagarajan KP, Morris-Thomas MT. Simulation of the dam break problem and impact flows using a Navier-Stokes solver. Simulation 2004;13:17.

[28] Daneshfaraz R, Minaei O, Abraham J, Dadashi S, Ghaderi A. 3-D Numerical simulation of water flow over a broad-crested weir with openings. ISH J Hydraul Eng 2019:1–9. doi:10.1080/09715010.2019.1581098.

[29] Li G, Li P, Li X, Deng Y. Numerical optimization of oblique cut bucket and its application in Ski jump of Shiziya dam. ISH J Hydraul Eng 2019:1–10. doi:10.1080/09715010.2019.1685915.

[30] Flow Science Inc. FLOW-3D User's Manual. 9.3 ed. Flow Science Inc, Los Alamos 2008. n.d.

[31] Ozmen-Cagatay H, Kocaman S, Guzel H. Investigation of dam-break flood waves in a dry channel with a hump. J Hydro-Environment Res 2014;8:304–15. doi:10.1016/j.jher.2014.01.005.

[32] Kocaman S, Ozmen-Cagatay H. Investigation of dam-break induced shock waves impact on a vertical wall. J Hydrol 2015;525:1–12. doi:10.1016/j.jhydrol.2015.03.040.

[33] Zhou Z, Wang X, Chen W, Deng S, Liu M. Numerical Simulation of Dam-Break Flooding of Cascade Reservoirs. Trans Tianjin Univ 2017;23:570–81. doi:10.1007/s12209-017-0073-y.

[34] Hu H, Zhang J, Li T. Dam-Break Flows: Comparison between Flow-3D, MIKE 3 FM, and Analytical Solutions with Experimental Data. Appl Sci 2018;8:2456. doi:10.3390/app8122456.

[35] Tahershamsi A, Hooshyaripor F, Razi S. Reservoir's Geometry Impact of Three Dimensions on Peak-Discharge of Dam Failure Flash Flood. Sci Iran 2017:0–0. doi:10.24200/sci.2017.4467.

[36] Harlow FH. Turbulence Transport Equations. Phys Fluids 1967;10:2323. doi:10.1063/1.1762039.